scientific reports

Check for updates

OPEN

Hydroxyl radical production in liquid water by laser cavitation

Xinxin Zhou & Jiayang Gu✉

Laser cavitation (LC) is an interesting novel method to the production of hydroxyl (·OH) radical. A setup of LC system was designed and methylene blue (MB) aqueous solution was chosen to detect the ·OH radical. The production and detection mechanism of ·OH radical were investigated combined with the evolution process of laser-induced cavitation bubble. The effects of operating parameters (laser energy, pulse frequency, temperature, pH value, water matrix and liquid state) on the production were discussed. Moreover, the energy consumption of LC was analyzed. The results indicate that the production of ·OH radical origins from the tearing of water molecules by the combined impact of laser shock wave, bubble collapse shock wave and water-jet, and the optimal concentration of MB is 5 mg/L. The production yield of ·OH radical increases with the rise of laser energy (25 mJ – 150 mJ) and pulse frequency (1 –5 Hz). The optimal temperature for the production yield is ranging from 35 ℃ to 45 ℃, and the conditions of flowing, acidic tap water are more conducive to the production of ·OH radical. The production of ·OH radicals by LC at 25 mJ laser energy and 1 Hz pulse frequency have the best production efficiency.

Keywords Laser cavitation, Hydroxyl radical, Cavitation bubble, Operating parameter, Energy consumption

Nowadays, cavitation technology in advanced oxidation processes has been applied in the field of organic wastewater degradation and presents the broad prospects[1–3]. The oxidation of hydroxyl radical is the main mechanism of cavitation degradation of organic wastewater. Due to the extreme environment of high temperature and high pressure in the process of cavitation bubble collapse[4], the water molecules are dissociated and thereby causing the production of hydroxyl radical. Hydroxyl (·OH) radical, a radical with strong oxidizing ability (oxidation potential is 2.81 V), has the characteristics of high activity and fast reaction rate[5–7]. It can react with various organic compounds and oxide them into carbon dioxide, water and other harmless substances through the electron transfer, electrophilic addition, dehydrogenation reaction and other ways[8,9].

Cavitation is a unique phenomenon that occurs when the internal temperature of the liquid is higher than the saturated vapor temperature under normal pressure or the local pressure inside the liquid drops[10]. Cavitation can usually be divided into four kinds of acoustic, hydraulic, optical and particle cavitation. At present, the research on the production of •OH radical mainly focus on hydraulic cavitation and acoustic cavitation. Didenko et al.[11] quantitatively detected the hydroxyl radical content in sonochemistry reactions by collecting SBSL spectra in water of a single bubble at 28 kHz and 52 kHz, and at 3℃ and 22℃, respectively. Merouani et al.[12] developed a simple semi-empirical method to predict the number of active bubbles and using a model that combines the bubble dynamics with a chemical kinetics model in acoustic field to predict the chemical yield (particularly, the amounts of $\cdot OH$, $HO_2\cdot$ and H_2O_2) produced by single bubble. Rehman et al.[13] compared the free radicals formation induced by cold atmospheric plasma, ultrasound, and ionizing radiation. The similarities and differences between the plasma chemistry, sonochemistry, and radiation chemistry are explained. Takahashi et al.[14] investigated the generation of free-radical from collapsing micro-bubbles in the absence of a dynamic stimulus. It demonstrated that the generation of free radicals is due to the extremely high temperature caused by adiabatic compression during violent collapse.

The incident laser radiation triggers a complex interplay between the chemical and physical processes at the interface between the solid surface and the liquid or gas environment[15]. Laser cavitation (LC) is a novel method for studying the phenomenon of cavitation, which attracts much attention because of the advantages of easy to control, remote operation and non-contact[16]. When the pulse laser beam is focused on the liquid, the water will broke down and form a plasma. The pressure near the laser region increases sharply and expands outward, which cause the pressure inside the gas cavity to drop sharply and the generation of cavitation bubble[17]. Pawlak et al.[18] investigated the hydrogen production in liquid water by femtosecond laser-induced plasma and analyzed the energy efficiency of hydrogen production. Ren et al.[19,20] used the laser-induced cavitation bubbles to strengthen the surface of aluminum alloys and discussed the strengthening mechanisms. However, few studies have been

School of Intelligent Manufacturing, Jiangsu College of Engineering and Technology, Nantong 226001, P.R. China. ✉email: jsgcxy_gjy@163.com

reported on the production of ·OH radical in liquid water by LC, and no relevant researches have mentioned that the effects of operating parameters on LC. Timberlake et al.[21] detected ·OH radical production by Nd: YAG laser photodisruption, but the study was conducted in the context of ophthalmic applications and did not systematically investigate the influence of laser energy, pulse frequency, temperature, pH, or water matrix on ·OH yield. Liu et al.[22] used a liquid-jet produced by the collapse of a laser-induced bubble to investigate the effect of cavitation on the copper target. The results indicated that the liquid-jet impact is the main damage mechanism in cavitation erosion. Zhang et al.[23] used a high-speed camera to study the collapsing dynamics of a laser-induced cavitation bubble near the edge of a rigid wall. It was found that the bubble would gradually approach the edge in the pulsation, and the generation distance of the bubble had a great influence on the bubble evolution. Pawlak et al.[24] investigated hydrogen production in liquid water by femtosecond laser-induced plasma, but focused on hydrogen yield rather than ·OH radical detection or parametric optimization.

In this study, a setup of LC was designed to investigated production of ·OH radical. MB aqueous solution was employed to detect the content of produced ·OH radical. The production and detection mechanism of ·OH radical were investigated combined with the evolution process of laser-induced cavitation bubble. The effects of operating parameters including laser energy, pulse frequency, temperature, pH value, water matrix and liquid state on the production were discussed. Finally, the energy consumption of LC used to produce ·OH radical was analyzed.

Experiment

Reagents and testing instruments

Experimental reagents: Methylene blue (MB, molecular formula: $C_{16}H_{18}ClN_3S$; molecular weight: 319.85 g·mol^{-1}; chemical class: thiazine), purchased from Shanghai maikun chemical co. LTD., China. Sulfuric acid (H_2SO_4, purchased from Yangzhou Hubao Chemical Reagent Co., Ltd.). Sodium hydroxide (NaOH, purchased from Shanghai Wokai Biotechnology Technology Co., Ltd.). All the reagents are analytical reagent grade and can be used without further purification.

Testing instrument: ultraviolet (UV) spectrophotometer (Cary 8454 UV-Vis, Agilent), electronic balance (Sartorius Technology (Beijing) Co., Ltd.) and pH test pen (Taiwan heng xin co., Ltd.).

Experimental setup

The experimental setup of LC system includes a nanosecond laser generator (Nd: YAG dual-wavelength solid-state laser, 1064 nm wavelength and 8 ns pulse width, Kinder Optoelectronics Technology Co., Ltd.), lens group (reflector lens, concave lens and convex lens), laser energy meter (NIM-E1000, China Institute of Metrology), three-dimensional mobile platform (SIMUMEIK-840Di, SIMENS), Collection type constant temperature heating magnetic stirrer (DF-101 S, Shanghai Chen bang xi instrument technology co., Ltd.), high-speed camera (V2512-144G, Phantom, USA) and laser light source (Cavitar, Finland).

Figure 1 depicts the experimental system of LC degradation. A computer-controlled Q-switched Nd: YAG laser generator is employed to induce cavitation bubble. The pulsed laser beam generates in the horizontal direction and is reflected by a 45-degree lens to the vertical direction. Then this laser beam is diverged by a concave lens and converted into parallel light by a convex lens. Finally, the laser beam is focused by the other convex lens on

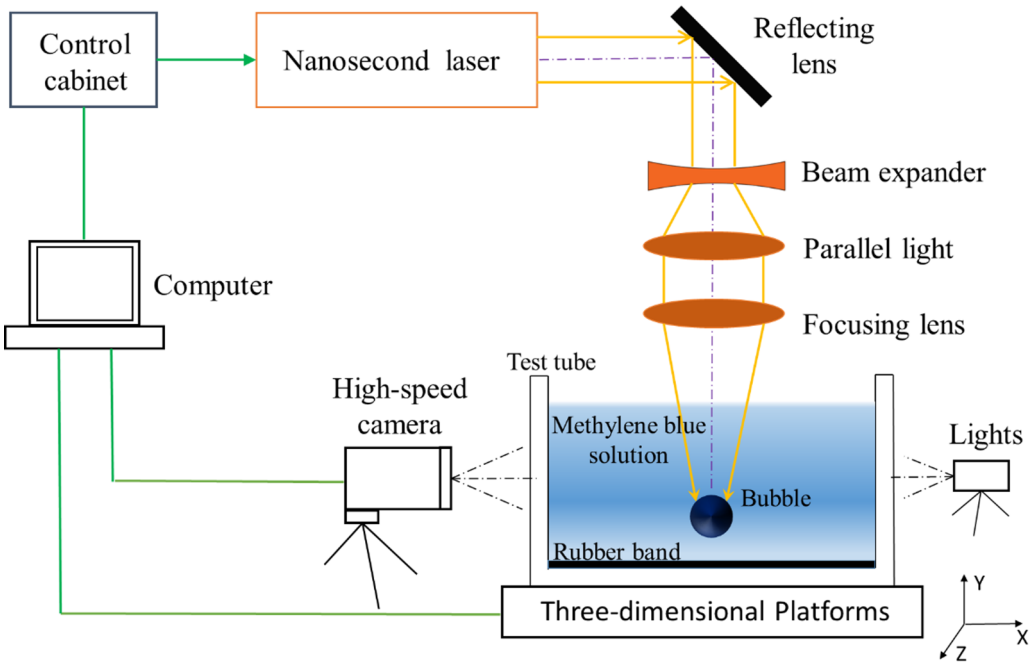

Fig. 1. Schematic representation of the experimental system.

the MB solution. The MB solution is in the test tube and the test tube is placed on the working platform. The black rubber ring is on the bottom of test tube so as to absorb laser energy and improve the efficiency of LC. The focus of laser beam is 1 mm above on the rubber ring through the adjustment of three-position mobile platform. Additionally, the dynamic sequence snapshots of laser-induced cavitation bubbles were recorded using a high-speed camera operating at a frame rate of 200,000 frames per second (fps), corresponding to a time interval of 5 μs between consecutive frames.

Experimental and analytical procedure

In the experiment, MB was adopted as a detection agent for ·OH radical. MB aqueous solution was prepared with tap water and deionized water, and the solution used to the experiment was 6 mL. The production of ·OH radical by LC was carried out at various operating parameters including laser energy (25 mJ, 50 mJ, 75 mJ, 100 mJ, 125 mJ and 150 mJ), pulse frequency (1 Hz, 2 Hz, 3 Hz, 4 Hz and 5 Hz), temperature (15 ℃, 25 ℃, 35 ℃, 45 ℃, 55 ℃ and 65 ℃), pH value (2, 4, 6, 8, 10 and 12), water matrix and flow condition. For each kind of MB aqueous solution sample, the experiment time was respectively 10 min, 20 min, 30 min, 40 min, 50 min and 60 min. All the experiments were repeated three times and averaged.

Based on Lambert-Beer's law[25], the concentration (C) change of MB solution was obtained through the measurement of the absorbance (Abs) of MB solution at the maximum absorption wavelength of 664 nm. The content of ·OH radical was determined through chemical reaction between MB and ·OH radicals. The absorbance of various MB concentrations was determined by UV spectrophotometer, and the standard curve of MB concentration-absorbance was set up to obtain the linear equation with a correlation coefficient $R^2 = 0.9994$, as shown in Eq. (1).

$$Abs = 0.10364C + 0.00376 \tag{1}$$

The concentration of ·OH radical can be calculated according to Eq. (1), as shown in Eq. (2):

$$C_{\bullet\,\mathrm{OH}} = C_{\mathrm{MB1}} - C_{\mathrm{MB2}} = \frac{A_1 - A_2}{0.10364} \tag{2}$$

where C_{MB1} and C_{MB2} are the concentration of MB in the solution before and after the LC treatment, mg/L; A_1 and A_2 represent the absorbance value of the solution before and after the experiment, respectively.

The production of ·OH radical can be obtained from the Eq. (3):

$$n = (C_{\bullet\,\mathrm{OH}} * V)/M \tag{3}$$

where n is the quantity of ·OH radical, μ mol; $C_{\bullet\,\mathrm{OH}}$ is the concentration of ·OH radical, mg/L; L is the volume of MB solution, mL; M is the molar mass of ·OH radical, g·mol^{-1}.

Results and discussion

Production and detection mechanism of ·OH radical

Bubble evolution and •OH radical production

The process of LC is complicated compared to other cavitation methods, so the production mechanism of ·OH radicals by LC was investigated combined with the evolution details of laser-induced cavitation bubble. The dynamic sequent snapshots of laser-induced cavitation bubble were recorded by a high-speed camera at a rate of 200,000 frames per. Figure 2 shows the bubble evolution details during the three pulsation process, and the time interval between each frame is 10 μs. When the focused laser beam is incident to the MB solution, the liquid will be breakdown and a plasma forms accompanied by the environment of high-temperature and high-pressure if the laser power density exceeds the breakdown threshold of the solution[26–28]. Due to the absorption of laser energy, the plasma accelerates to expand and become a cavitation bubble. In the first pulsation period, the bubble experiences 130 μs from initial birth to maximum radius and the process of contraction to collapse is from 130 μs to 220 μs. Most of the bubble energy is consumed in the first pulsation, so the pulsation period and maximum radius of cavitation bubble significantly decreases in the second pulsation, and the shape of bubble become flat[29]. The pulsation period and maximum radius of bubble further decrease in the third pulsation.

It is important to note that laser-induced optical breakdown in water generates not only ·OH radicals but also other transient species, including hydrated electrons (e^-_{aq}), hydrogen atoms (·H), and superoxide radicals (O_2^{-}·). While MB is primarily used as a ·OH probe, it may also react with reducing species, leading to potential underestimation or overestimation of ·OH yield. Future work employing selective probes (e.g., terephthalic acid for ·OH) is recommended to quantify ·OH radicals more accurately.

Figure 3 shows the process of water molecules tearing and production of ·OH radical by LC. The laser shock wave generates when the liquid is breakdown by the focused laser beam and thereby the water molecules are torn. Then the plasma expands to a cavitation bubble and the bubble undergoes the periodic pulsation of "expansion and contraction". The high-intensity shock wave and water-jet generate when the cavitation bubble collapses in the first pulsation, so the water molecules are torn again. Suslick et al.[30] reported that the instantaneous temperature can reach 1900 K and the local pressure can reach up to 5.05KPa as the bubble collapses, which is much higher than the chemical bond of water molecules. Due to large quantity of bubble energy is consumed in the first pulsation, the intensity of bubble collapse shock wave and water-jet in the second pulsation is weak, and the production yield of ·OH radical is relatively low. In the third pulsation, the shock wave and water-jet are weaker and the production of ·OH radical can be ignored. Although the process of laser breakdown and bubble collapse is very short, it is enough to complete the tearing of water molecules and the production of ·OH radical.

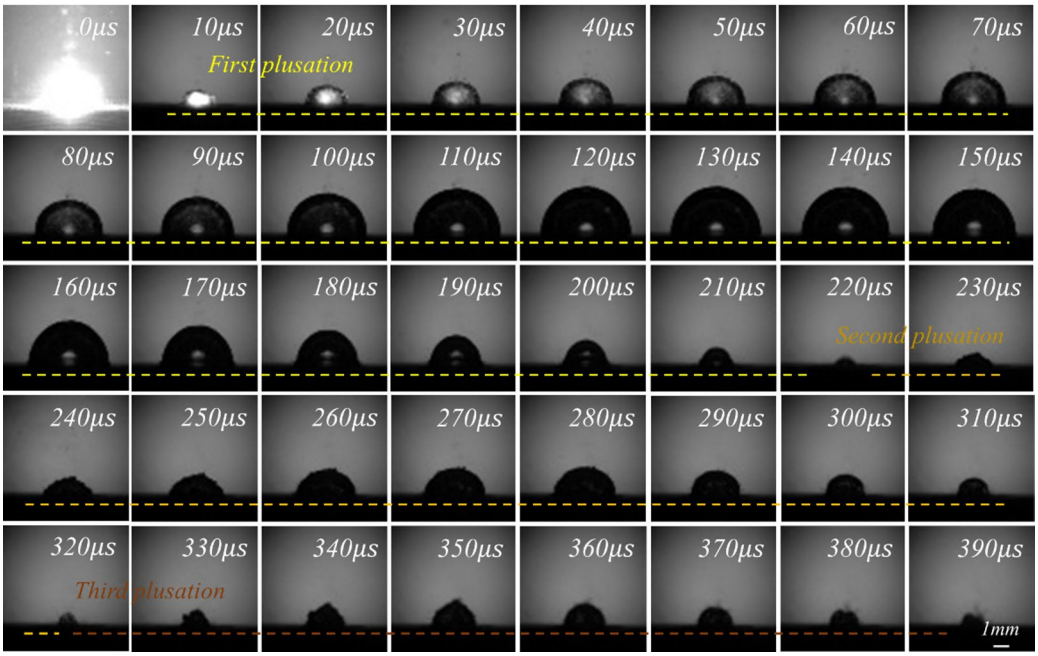

Fig. 2. The dynamic sequence snapshots of laser-induced cavitation bubble during the three pulsation period.

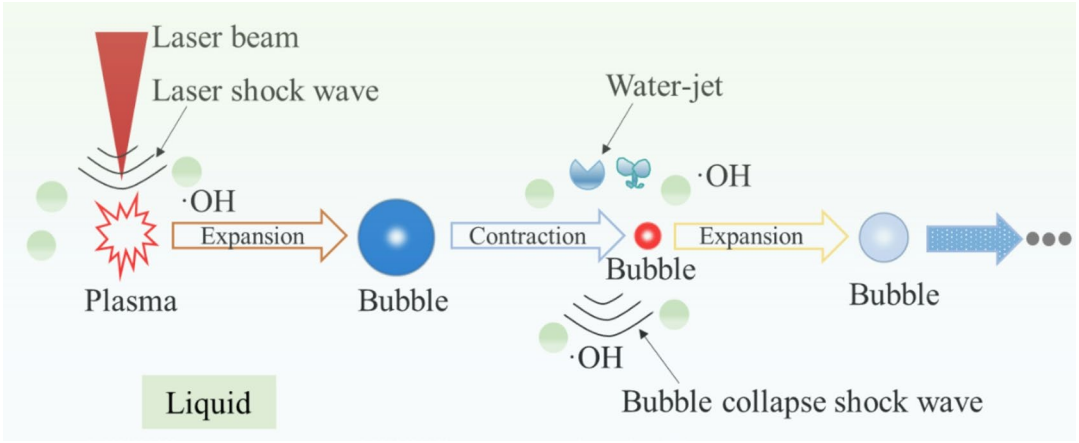

Fig. 3. Schematic representation of production of ·OH radical by LC.

However, if LC lasts for a long time continuously, ·OH radical will self-react or reacts with the ·H radicals and other generated molecules. A series of reactions during the LC can be described as follow:

$$H_2O \rightarrow {}^{\bullet}OH + {}^{\bullet}H \tag{4}$$

$${}^{\bullet}OH + {}^{\bullet}OH \rightarrow H_2O_2 \tag{5}$$

$${}^{\bullet}OH + {}^{\bullet}H \rightarrow H_2O \tag{6}$$

$${}^{\bullet}OH + H_2O_2 \rightarrow H_2O + HO_2 \tag{7}$$

While previous studies have confirmed the occurrence of ·OH radicals during laser-induced breakdown or cavitation[31], the present work provides, for the first time, a direct correlation between the dynamic evolution of the laser-induced cavitation bubble (first, second, and third pulsations) and the temporal production profile of ·OH radicals. Furthermore, we demonstrate that the combined impact of the laser shock wave, bubble collapse shock wave, and water-jet constitutes the primary mechanical–chemical energy conversion pathway for water molecule dissociation. This mechanistic interpretation extends beyond previous reports, which primarily attributed radical formation solely to the high-temperature, high-pressure environment during bubble collapse.

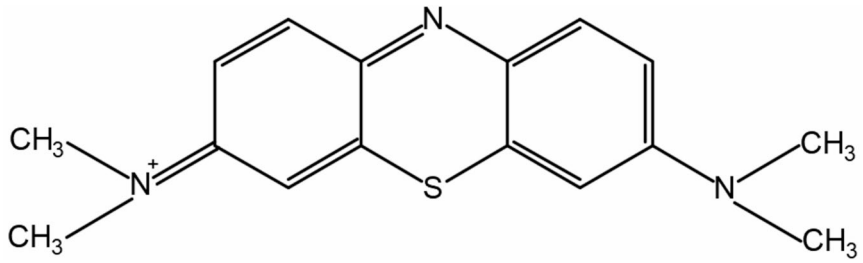

Fig. 4. Chemical structure of MB.

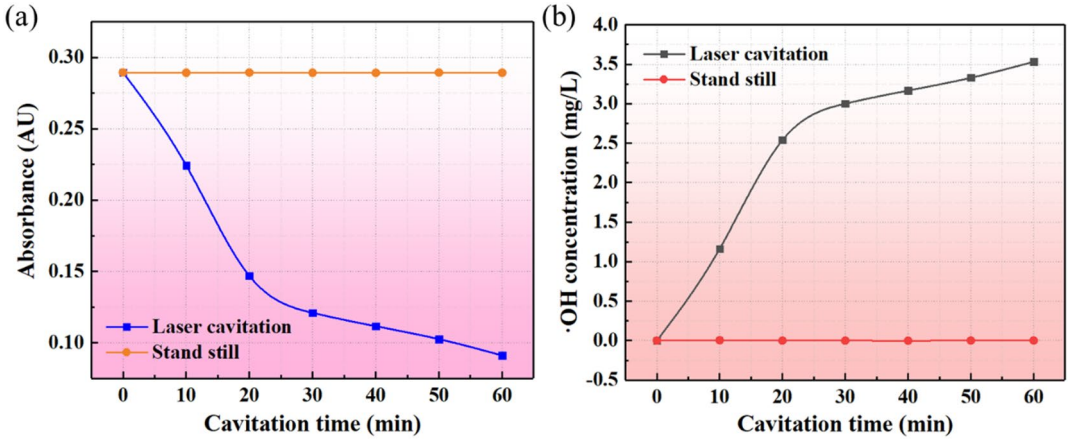

Fig. 5. Change curve of (**a**) absorbance and (**b**) the concentration of ·OH radical with cavitation time.

Determination of MB and ·OH radicals

MB is a thiazine-type reagent, which molecule contains a dibenzothiothiazine ring system, and the sulfur atom is in the intermediate valence state[32–34], and the chemical structural is shown in Fig. 4. MB has a high affinity for ·OH radical and can react with ·OH radical to form the oxidation product, hydroxylated methylene blue (MB-OH), as shown in Eq. (8). As the valence of sulfur increases after oxidation, MB loses its chromophore and gradually fades, and the blue color of MB aqueous solution will become lighter or even disappear. MB undergoes a rapid reaction with the ·OH radical, with an overall rate constant of 5.51×10^9 to 2.38×10^{10} M^{-1} s^{-1} and has a rather broad lifetime range .The initial hydroxylation of the phenothiazine ring at the C–S*=C position. The subsequent cleavage of the central sulfur-containing ring and formation of sulfoxide intermediates. Further oxidation leading to ring-opening reactions and eventual mineralization to CO_2, H_2O, and inorganic ions[35]. The high valence sulfur is more difficult to be reduced, so the reaction product MB-OH has good stability.

$$^{\bullet}OH + MB \rightarrow MB - OH \tag{8}$$

The comparative experiment was conducted so as to determine the effect of production of ·OH radical by LC. Figure 5(a) and (b) shows the changes in absorbance and ·OH radicals production with LC treatment and standing still MB solution as a function of cavitation time, respectively. When the MB solution is standing still, the absorbance has no change and there are no ·OH radical produces. After LC treatment, the absorbance of MB solution decreases and the concentration of ·OH radical increases significantly, which verifies that LC can produce ·OH radicals in liquid water. It can be seen that the concentration of ·OH radical increases rapidly during the 20 min cavitation time while it increases become slowly and stabilized as the further increase of cavitation time.

Control UV-Vis spectra showed no evidence of MB dimer formation (characteristic absorption at 605 nm) under our experimental conditions, confirming that MB remains monomeric at the concentrations used. Potential dimerization of oxidized MB products, while theoretically possible, is not expected to significantly influence the measured absorbance at 664 nm. In addition to the collision probability argument, the decrease in detected ·OH yield at MB concentrations above 5 mg/L may also be attributed to competitive photon absorption. At high laser intensities, MB may undergo two-photon absorption of the 1064 nm laser radiation, leading to direct photodegradation or excited-state reactions that do not involve ·OH radicals. This would reduce the apparent ·OH yield as measured by MB decolorization. Furthermore, high MB concentrations may attenuate the laser beam before it reaches the focal point, reducing the efficiency of optical breakdown and cavitation generation. These factors collectively contribute to the observed optimal MB concentration of 5 mg/L.

The MB concentration of solution is a non-negligible condition in the production of ·OH radical by LC. It is important to determine the most suitable concentration of MB solution for capturing ·OH radical. The various concentration (1, 2, 3, 4, 5, 6, 7, 8 mg/L) MB solutions were prepared, and the experiments were performed under the condition of 100 mJ laser energy, 2 Hz pulse frequency and 25 ℃ temperature. As shown in Fig. 6, the detected ·OH yield increases with MB concentration up to 5 mg/L, beyond which it declines. This non-monotonic behavior can be attributed to several competing factors: (1) At low MB concentrations (< 5 mg/L), the reaction rate is limited by the collision frequency between ·OH radicals and MB molecules. Increasing MB concentration enhances the probability of ·OH capture, leading to higher detected yield. (2) At the optimal concentration (5 mg/L), the system achieves a balance between sufficient MB availability and efficient cavitation generation. (3) At excessively high MB concentrations (> 5 mg/L), the following detrimental effects emerge: Optical attenuation: High MB concentration absorbs and scatters the incident laser beam, reducing the effective laser energy reaching the focal point and thus decreasing cavitation intensity. Competitive photon absorption: MB may undergo multiphoton absorption, leading to direct photodegradation that does not involve ·OH radicals. Inner filter effect: The high absorbance of the solution re-absorbs the UV-Vis measurement beam, leading to an underestimation of MB decolorization and thus an apparent decrease in ·OH yield. Therefore, the observed decrease in detected ·OH yield at high MB concentrations does not indicate a true reduction in ·OH production, but rather reflects optical and photochemical artifacts that limit the accuracy of MB as a ·OH probe under such conditions. Therefore, the optimal ·OH radical detection effect is obtained when the initial MB concentration is 5 mg/L.

The apparent ·OH production yield is governed by the competition between several parallel reactions, as shown in Eq. (4)(5)(6)(7). The rate constants of the chemical reactions are $k_1 \approx 3.5 \times 10^9$ $M^{-1}s^{-1}$, $k_2 \approx 5.5 \times 10^9$ $M^{-1}s^{-1}$, $k_3 \approx 7.0 \times 10^9$ $M^{-1}s^{-1}$, $k_4 \approx 2.7 \times 10^7$ $M^{-1}s^{-1}$ respectively. At low MB concentrations, radical–radical recombination reactions (Eq. (5)(6)) dominate, leading to low ·OH utilization efficiency. As MB concentration increases, Eq. (4) becomes increasingly competitive, and more ·OH radicals are trapped by MB molecules, resulting in a higher detected yield. However, beyond the optimal concentration (5 mg/L), the solution becomes optically dense, reducing cavitation efficiency, and MB self-quenching or direct photolysis may occur. Additionally, the accumulated H_2O_2 from Eq. (5) may act as a ·OH scavenger via Eq. (7) at longer cavitation times.

Effect of operating parameters

Laser energy

Laser energy is a key parameter for the production of ·OH radical by LC. The effect of laser energy on the production of ·OH radical was investigated at various laser energies of 25 mJ, 50 mJ, 75 mJ, 100 mJ, 125 mJ and 150 mJ, and the production yield for 60 min are shown in Fig. 7. The other experimental conditions were 2 Hz pulse frequency, 25 ℃ temperature and 5 mg/L MB concentration. It can be observed from Fig. 7(a) that the production yield of ·OH radical increase with the rise of laser energy, and the amount of substance are respectively 0.794, 0.894, 1.118, 1.247, 1.347 and 1.506 μmol at six kids of laser energies. Figure 7(b) shows the production velocity of ·OH radical as a function of cavitation time at various laser energies. Similarly, the production velocity is higher under higher laser energy in each time period. However, the cavitation time for reaching maximum production velocity is different at various laser energies. At 25 mJ and 50 mJ, the production velocity is relatively lower and the maximum velocity occur in 30 min. The production velocity increases obviously with the rise of laser energy. The maximum velocity at 75 mJ and 100 mJ appear in 20 min while it at 125 mJ and 150 mJ are in 10 min. The production of ·OH radical can be attributed to the tearing of water molecules by the combined impact of laser shock wave, bubble collapse shock wave and water-jet. On the one hand, the extent of optical breakdown and the laser shock wave become more and more intense with increasing the laser energy, so more water molecules will be torn under higher laser energy. On the other hand, the maximum radius of cavitation bubble increases with the rise of laser energy[36,37], and the bubble energy is proportional to the cube of its maximum radius[38,39], so the cavitation bubble has higher bubble energy under higher laser energy. The

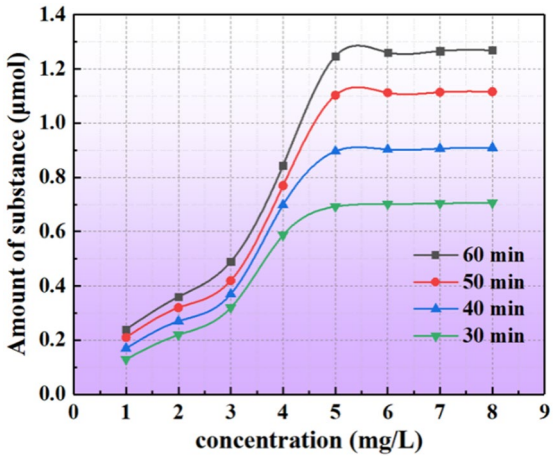

Fig. 6. Relationship between detected ·OH radical production and the initial concentration of MB solution.

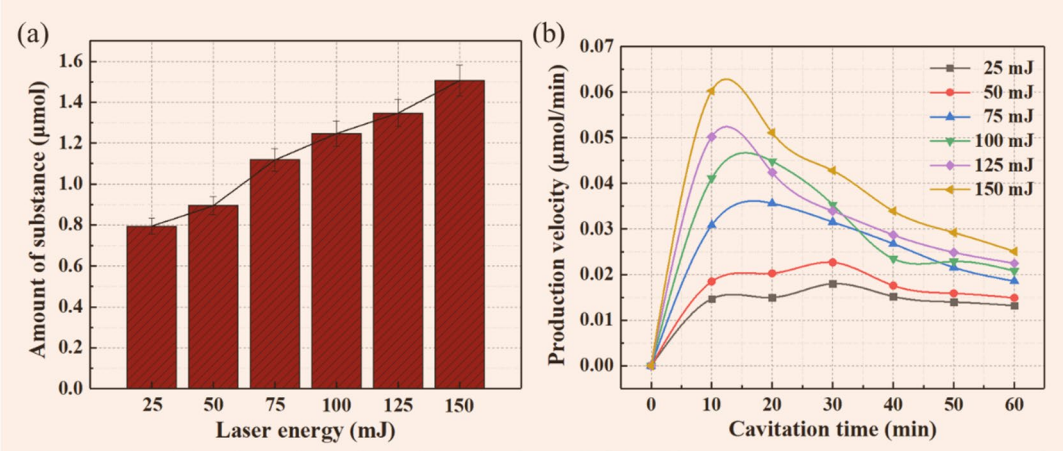

Fig. 7. (**a**) Production yield of ·OH radicals by LC under various laser energies, (**b**) production velocity of ·OH radical as a function of cavitation time under various laser energies.

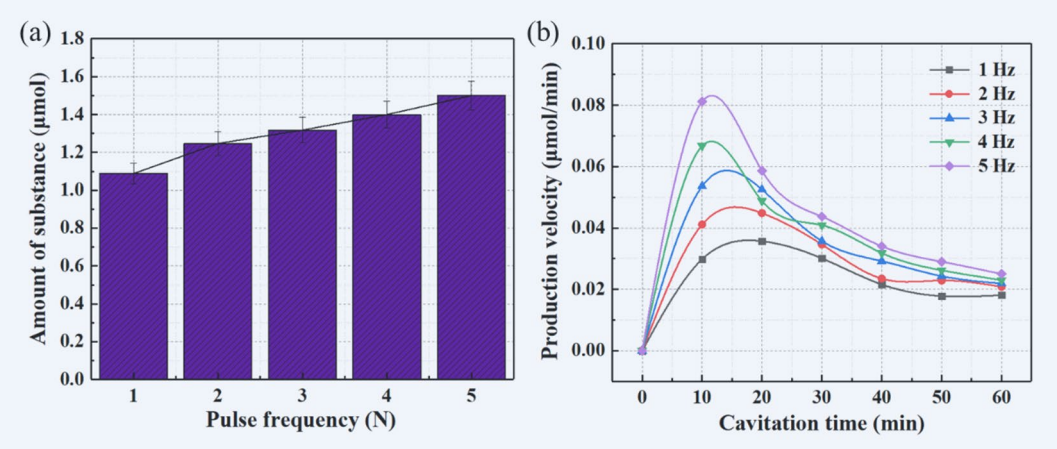

Fig. 8. (**a**) Production yield of ·OH radical by LC under various pulse frequencies, (**b**) production velocity of ·OH radical as a function of cavitation time under various pulse frequencies.

intense of shock wave and water-jet is higher when the bubble collapses at higher laser energy, so the water molecules are more likely to be torn and the reaction opportunity of ·OH radicals and MB molecules increase.

Pulse frequency

Pulse frequency is also an important parameter in LC. The effect of pulse frequency on the production of ·OH radical was investigated at various pulse frequencies of 1 Hz, 2 Hz, 3 Hz, 4 Hz and 5 Hz. All experiments were conducted in 5 mg/L MB solution, 100 mJ laser energy and 25 ℃ temperature. Figure 8(a) shows the production yield of ·OH radical by LC treatment for 60 min, and the amount of substance at five frequency are 1.088, 1.247, 1.318, 1.405, 1.513 μmol, respectively. In Fig. 8(b), the production velocity of ·OH radicals increase firstly and then decrease as cavitation progresses, and the production velocity is higher under higher pulse frequency. The production velocity reaches the maximum value in 10 min under 4 Hz and 5 Hz, while it decreases significantly as the increase of cavitation time. At 1 Hz and 2 Hz, the production velocity always increases during the 20 min cavitation time. The increase in pulse frequency causes the breakdown of MB solution by LC for multiple times, which accelerates the production of ·OH radicals and increases the collision probability of MB molecule and ·OH radical. The time interval between pulses is short, so an increase in pulse frequency is almost equivalent to an increase in laser energy in the certain extent. Therefore, the trend of production yield and velocity of ·OH radical at various pulse frequencies are similar to that at various laser energies.

Temperature

The effect of temperature (15 ℃, 25 ℃, 35 ℃, 45 ℃, 55 ℃ and 65 ℃) in 5 mg/L MB solution on the production of ·OH radical was investigated, and the results are presented in Fig. 9. The laser energy and pulse frequency were kept at 100 mJ and 2 Hz, and the method of water bath heating was adopted to maintain the constant temperature of MB solution. Figure 9(a) shows the production yield of ·OH radical under various temperatures after 60 min

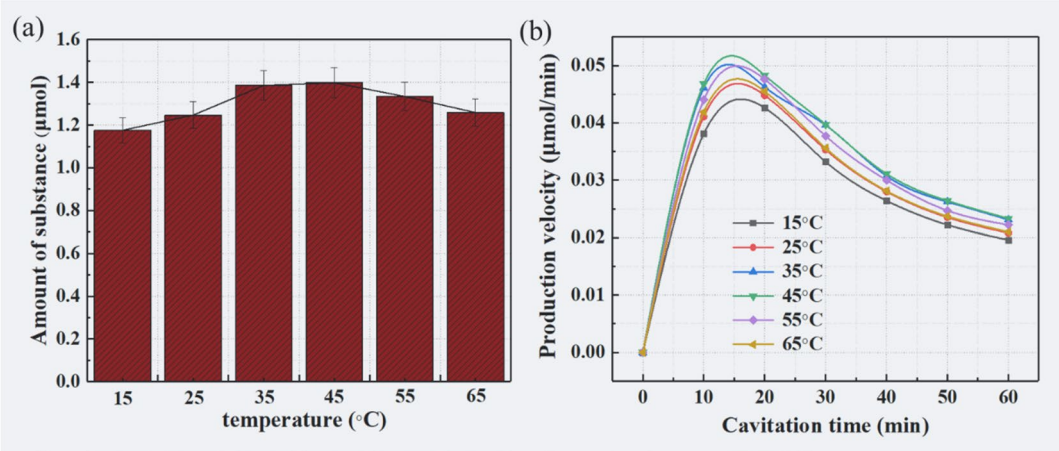

Fig. 9. (**a**) Production yield of ·OH radical by LC under various temperatures, (**b**) production velocity of ·OH radical as a function of cavitation time under various temperatures.

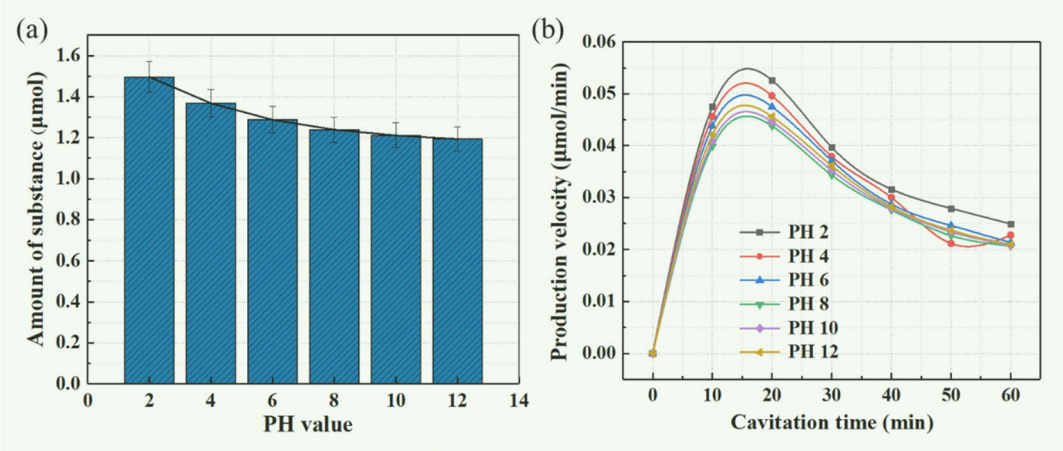

Fig. 10. (**a**) Production yield of ·OH radical by LC under various pH values, (**b**) production velocity of ·OH radical as a function of cavitation time under various pH values.

LC treatment, and Fig. 9(b) shows the production velocity of ·OH radicals as a function of cavitation time at various temperatures. It can be seen that the amount of substance increases from 15 ℃ to 45 ℃ temperature while it decreases when the temperature rises to 55 ℃ and 65 ℃, so the optimal temperature for the production of ·OH radical ranges from 35 ℃ to 45 ℃. The change of production velocity at each temperature is not very obvious and has a good consistency, and the maximum production velocity all appear in about 15 min. The viscosity, surface tension and saturated vapor pressure of the liquid will change if the solution temperature changes, so the effect of temperature is complicated[40]. The maximum radius of cavitation bubble increases with the rise of temperature, and the bubble energy and pulsation period increase with increasing the maximum radius of bubble[41,42]. Therefore, the intense of shock wave as well as water-jet is higher when the bubble collapses under higher temperature, and the water molecule is more likely to be torn apart to produce ·OH radical. Moreover, the higher the temperature, the more intense the random movement of MB molecules, so the MB molecules are more likely to diffuse to the water-bubble interface at higher temperature and react with ·OH radicals. Kavitha and Sun et al.[43,44] also reported that the increase in temperature can result in an increase in the production of ·OH radical. However, excessively high temperature is detrimental to the production of ·OH radical. The intensity of cavitation decreases with rising the temperature because of the less violent collapse of the formed gas cavity[45,46].

pH value

The effect of pH value on the production of ·OH radical was investigated at various pH values ranging from 2 to 12. All experiments were performed in the condition of 100 mJ laser energy, 2 Hz pulse frequency, 25 ℃ temperature and 5 mg/L MB solution. It can be seen from Fig. 10(a) that the production yield of ·OH radical decreases with the pH value increases from 2 to 8, and it almost keeps unchanged at the range of pH8 to pH12. The amount of substance is higher in acidic solution while it does not have obvious differences in neutral and

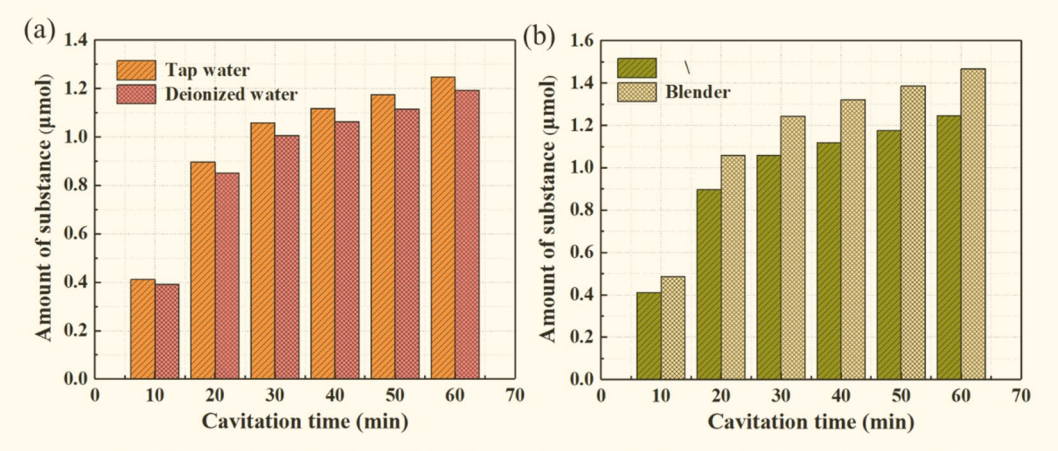

Fig. 11. Production yield of ·OH radical by LC under various (**a**) water matrix and (**b**) flow state as a function of cavitation time.

Laser energy (mJ)	Pulse frequency (Hz)	Production yield (μmol)	Power density (J/mL)	energy efficiency (μmol /(J/mL))
25	2	0.794	30	0.0265
50	2	0.894	60	0.0149
75	2	1.118	90	0.0124
100	2	1.247	120	0.0104
125	2	1.347	150	0.0090
150	2	1.506	180	0.0084
100	1	1.088	60	0.181
100	3	1.318	180	0.0073
100	4	1.405	240	0.0059
100	5	1.513	300	0.0050

Table 1. The energy efficiency at various laser energies and pulse frequencies.

alkaline solutions. Figure 10(b) shows the production velocity of ·OH radical as a function of cavitation time at various pH values. The production velocity increases firstly and reaches the maximum value at about 15 min, and then it decreases with the as the cavitation time increases. The acidic conditions are more conducive to the production of ·OH radical and the produced ·OH radical does not readily self-react to form H_2O_2[47,48]. Moreover, the oxidation potential of ·OH radical increases and the physical properties of MB molecule changes in acidic solution. The effect of neutral and alkaline conditions are almost the same, and ·OH radical can be converted into O- in strongly alkaline solutions. In acidic conditions (pH 2–4), MB exists predominantly in its protonated form, which is more electrophilic and thus more susceptible to ·OH attack. Additionally, ·OH radicals have a higher oxidation potential at low pH, and their recombination to H_2O_2 is suppressed, leading to higher steady-state ·OH concentrations. In neutral conditions (pH 6–8), MB is partially protonated, and ·OH recombination becomes more favorable, resulting in moderate degradation efficiency. In alkaline conditions (pH 10–12), we now explain that: (a) a portion of ·OH is scavenged by OH^- to form the less reactive O^-· species, (b) MB is deprotonated and electronically stabilized, and (c) dissolved CO_2 may form carbonates/bicarbonates that act as ·OH scavengers. These factors collectively contribute to the observed lower ·OH detection yield.

A consistent trend observed across all parametric studies is that the ·OH production rate increases rapidly during the initial 10–20 min of cavitation, reaches a maximum, and then gradually declines. This behavior can be attributed to two competing factors: (1) the continuous generation of ·OH radicals via laser-induced cavitation, and (2) the simultaneous consumption of ·OH radicals through reactions with MB molecules and through radical–radical recombination (e.g., ·OH + ·OH → H_2O_2). In the early stage, the concentration of MB is high, and the collision frequency between ·OH and MB is maximal, leading to a high apparent production rate. As the reaction proceeds, MB concentration decreases, and the accumulated H_2O_2 may act as a ·OH scavenger. The system thus transitions from a MB-limited regime to a radical-recombination-limited regime, resulting in the observed peak and subsequent decline in production rate.

Water matrix and flow state

Water matrix and liquid state also have an influence on the production of ·OH radical. The effect of water matrix was investigated in tap water and deionized water, and the other experimental conditions unchanged. Figure 11(a)

shows the production yield of ·OH radical as a function of cavitation time in tap water and deionized water. It can be observed that the amount of substance increases with the increase of cavitation time, and the production yield is higher in tap water. It is well known that the liquid will not generate cavities without gas nuclei. There are few gas cores in deionized water, so the breakdown threshold of MB solution prepared by deionized water is high and it is hard to generate cavitation bubbles. Due to more ionic impurities and gas nuclei in tap water, the breakdown threshold is much lower than that of deionized water, which is conducive to the generation of cavitation bubbles.

The production of ·OH radical in the state of quiescent and flowing MB solution were investigated by using a magnetic stirrer to rotate the liquid in the container, and the results are shown in Fig. 11(b). It can be found that the production yield is higher in the case of rotation using a magnetic stirrer. In the case of quiescent MB solution, the breakdown of liquid and the production of ·OH radical only happen near the focus of laser, and many micro-bubbles attach to the black rubber ring will affect the penetration of laser hinder the production of ·OH radical. The flowing liquid can make the production of ·OH radical uniformly and stably, and the rubber ring wall is not easy to attach small bubbles.

Energy consumption analysis

The energy consumption of LC in the production of ·OH radical was analyzed. We define the parameter Q to describe the energy efficiency, which is described as the amount of produced ·OH radicals per unit power dissipation, as shown in Eq. (9).

$$Q = \text{Production yield}/\text{Power density} \tag{9}$$

where Q is the energy efficiency, μmol/(J/mL); Production yield is the amount of ·OH radical has produced by LC, μmol; power density, J/mL.

The power density can be defined by Eq. (10):

$$\text{Power density} = (P^{*}t) \ / \ V \tag{10}$$

where t is the cavitation time, s; V is the volume of MB solution, L; P is the power of pulse laser, w.

The power of pulse laser is represented by the following equation:

$$P = E^{*}f \tag{11}$$

where E is the energy of pulse laser, mJ; f is the pulse frequency of laser generator, Hz.

The energy efficiency at various laser energies and pulse frequencies are calculated and listed in Table 1. The energy efficiency is higher under the lower laser energy and pulse frequency. It can be induced that the best condition to produce ·OH radical by LC is 25 mJ laser energy and 1 Hz pulse frequency. Ref[49]. reported that the study of free radical production by Nd: YAG laser photodisruption. It used I^{3-} to detect the production yield of ·OH radical and concluded that 4×10^{-14} mol/mJ of ·OH radicals are produced at 100 mJ laser energy. In comparison, the production yield of ·OH radical is much higher and reaches 1.73×10^{-9} mol/mJ at 100 mJ laser energy in our study.

Conclusion

The production of ·OH radical in a self-designed LC system was reported. The production mechanism of ·OH radical can be attributed to the tearing of water molecules by the combined impact of laser shock wave, bubble collapse shock wave and water-jet in the process of laser breakdown and first pulsation. The ·OH radical was detected by MB aqueous solution and the optimal concentration of MB used is determined as 5 mg/L. The effects of operating parameters including laser energy, pulse frequency, temperature, pH value, water matrix and flow state on the production were revealed. The production yield of ·OH radical increases with the rise of laser energy (25 mJ − 150 mJ) and pulse frequency (1 −5 Hz). The optimal temperature for the production yield is ranging from 35 ℃ to 45 ℃, and the conditions of flowing (stirred), acidic tap water are more conducive to the production of ·OH radical. The energy consumption of LC in the production of ·OH radical was analyzed. The energy efficiency of ·OH radical production increases with the decrease of pulse energy and pulse frequency, and the best condition to produce ·OH radicals by LC is 25 mJ laser energy and 1 Hz pulse frequency. LC technology is considerable potential for both research and application, but there are still some shortcomings need to be improved in the subsequent studies.

Data availability

All data included in this paper are available upon request by contact with the corresponding author.

Received: 14 September 2025; Accepted: 17 February 2026
Published online: 27 February 2026

References

1. Cintas, P. & Luche, J. L. Green chemistry: the sonochemical approach. *Green. Chem.* **43**, 115–125. https://doi.org/10.1039/A900593E (1999).
2. Thanekar, P., Panda, M. & Gogate, P. R. Degradation of Carbamazepine Using Hydrodynamic Cavitation Combined With Advanced Oxidation Processes. *Ultrason. Sonochem*. **40**, 567–576. https://doi.org/10.1016/j.ultsonch.2017.08.001 (2018).

3. Gągol, M., Przyjazny, A. & Boczkaj, G. Wastewater treatment by means of advanced oxidation processes based on cavitation - A review. *Chem. Eng. J.* **338**, 599–627. https://doi.org/10.1016/j.cej.2018.01.049 (2018).
4. Kumar, P., Khanna, S. & Moholkar, V. S. Flow regime maps and optimization thereby of hydrodynamic cavitation reactors. *AIChE J.* **58**, 3858–3866. https://doi.org/10.1002/aic.13771 (2012).
5. Rajoriya, S., Bargole, S. & Saharan, V. K. Degradation of a cationic dye (Rhodamine 6G) using hydrodynamic cavitation coupled with other oxidative agents: Reaction mechanism and pathway. *Ultrason. Sonochem.* **34**, 183–194. https://doi.org/10.1016/j.ultsonch.2016.05.028 (2017).
6. Matilainen, A. & Sillanpaa, M. Removal of natural organic matter from drinking water by advanced oxidation processes. *Chemosphere* **80**, 351–365. https://doi.org/10.1016/j.chemosphere.2010.04.067 (2010).
7. Zhang, X. et al. Degradation of haloacetonitriles with UV/peroxymonosulfate process: Degradation pathway and the role of hydroxyl radicals. *Chem. Eng. J.* **364**, 1–10. https://doi.org/10.1016/j.cej.2019.01.029 (2019).
8. Cai, M. Q. et al. Decolorization of azo dyes Orange G using hydrodynamic cavitation coupled with heterogeneous Fenton process. *Ultrason. Sonochem.* **28**, 302–310. https://doi.org/10.1016/j.ultsonch.2015.08.001 (2016).
9. Qu, Y. N., Wu, J. W. & Meyer, J. R. Photoenhanced oxidation of nC60 in water: Exploring H_2O_2 and hydroxyl radical based reactions. *Chem. Eng. J.* **360**, 665–672. https://doi.org/10.1016/j.cej.2018.12.035 (2019).
10. Gogate, P. R. Cavitation: an auxiliary technique in wastewater treatment schemes. *Adv. Environ. Res.* **6**, 335–358. https://doi.org/10.1016/S1093-0191(01)00067-3 (2002).
11. Didenko, Y. T. & Suslick, K. S. The energy efficiency of formation of photons, radicals and ions during single-bubble cavitation. *Nature* **418**, 394. https://doi.org/10.1038/nature00895 (2002).
12. Merouani, S. et al. A method for predicting the number of active bubbles in sonochemical reactors. *Ultrason. Sonochem.* **22**, 51–58. https://doi.org/10.1016/j.ultsonch.2014.07.015 (2015).
13. Rehman, M. U. et al. Comparison of free radicals formation induced by cold atmospheric plasma, ultrasound, and ionizing radiation. *Arch. Biochem. Biophys.* **605**, 19–25. https://doi.org/10.1016/j.abb.2016.04.005 (2016).
14. Masayoshi, T., Kaneo, C. & Li, P. Free-Radical Generation from Collapsing Microbubbles in the Absence of a Dynamic Stimulus. *J. Phys. Chem. B.* **111** (6), 1343–1347. https://doi.org/10.1021/jp0669254 (2007).
15. Manshina, A. A. et al. The Second Laser Revolution in Chemistry: Emerging Laser Technologies for Precise Fabrication of Multifunctional Nanomaterials and Nanostructures. *Adv. Funct. Mater.* **40**, 2405457. https://doi.org/10.1002/adfm.202405457 (2024).
16. Zhang, Z., Wei, S., Wang, P., Qiu, W. & Zhang, G. Progress in applications of laser induced cavitation on surface processing, **170** 110212. (2024). https://doi.org/10.1016/j.optlastec.2023.110212
17. Cook, J. A., Gleeson, A. M., Roberts, R. M. & Rogers, R. L. A spark-generated bubble model with semi-empirical mass transport. *J. Acoust. Soc. Am.* **101**, 1908–1920. https://doi.org/10.1121/1.418236 (1997).
18. Pawlak, H. K. et al. Hydrogen production in liquid water by femtosecond laser-induced plasma. *Appl. Energ.* **247**, 24–31. https://doi.org/10.1016/j.apenergy.2019.04.010 (2019).
19. Ren, X. D. et al. Experimental investigation on dynamic characteristics and strengthening mechanism of laser-induced cavitation bubbles. *Ultrason. Sonochem.* **32**, 218–223. https://doi.org/10.1016/j.ultsonch.2016.03.012 (2016).
20. Ren, X. D. et al. Mechanical effect of laser-induced cavitation bubble of 2A02 alloy. *Opt. Laser Technol.* **105**, 180–184. https://doi.org/10.1016/j.optlastec.2018.02.039 (2018).
21. Timberlake, G. T., Gemperli, A. W., Larive, C. K., Warren, K. A. & Mainster, M. A. Free Radical Production by Nd: YAG Laser Photodisruption, Ophthal. *Surg. Las I.* **28**, 582–589. https://doi.org/10.3928/1542-8877-19970701-08 (2013).
22. Liu, X. M. et al. Effect of surface tension on a liquid-jet produced by the collapse of a laser-induced bubble against a rigid boundary. *Opt. Laser Technol.* **41**, 21–24. https://doi.org/10.1016/j.optlastec.2008.04.006 (2009).
23. Zhang, Y. N. et al. Collapsing dynamics of a laser-induced cavitation bubble near the edge of a rigid wall, **67** 105157. (2020). https://doi.org/10.1016/j.ultsonch.2020.105157
24. Pawlak, H. K., Tyczkowski, J., Jarota, A. & Abramczyk, H. Hydrogen production in liquid water by femtosecond laser-induced plasma. *Appl. Energ.* **247**, 24–31. https://doi.org/10.1016/j.apenergy.2019.04.010 (2019).
25. Bagal, M. V. & Gogate, P. R. Wastewater treatment using hybrid treat-ment schemes based on cavitation and Fenton chemistry: A review. *Ultrason. Sonochem.* **21**, 1–14. https://doi.org/10.1016/j.ultsonch.2013.07.009 (2014).
26. Putterman, S. J. & Weninger, K. R. Sonoluminescence: how bubbles turn sound into light. *Annu. Rev. Fluid Mech.* **32**, 445–476. https://doi.org/10.1146/annurev.fluid.32.1.445 (2000).
27. Xu, S. S. et al. Dependence of pulsed focused ultrasound induced thrombolysis on duty cycle and cavitation bubble size distribution. *Ultrason. Sonochem.* **22**, 160–166. https://doi.org/10.1016/j.ultsonch.2014.06.024 (2015).
28. Iii, M. N., Didenko, Y. T. & Suslick, K. S. Sonoluminescence temperatures during multi-bubble cavitation. *Nature* **401**, 772–775. https://doi.org/10.1038/44536 (1999).
29. Blake, J. R. et al. Interaction of two cavitation bubbles with a rigid boundary. *J. Fluid Mech.* **255**, 707–721. https://doi.org/10.1017/S0022112093002654 (2006).
30. Suslick, K. S., Gawienowski, J. J. & Schubert, P. F. Sonochemistry in non-aqueous liquids. *Ultrasonics* 33–36. https://doi.org/10.1016/0041-624X(84)90059-3 (1984).
31. Gu, J. Y. et al. Degradation of Rhodamine B in aqueous solution by laser cavitation. *Ultrason. Sonochem.* **68**, 105181. https://doi.org/10.1016/j.ultsonch.2020.105181 (2020).
32. Rauf, M. A. et al. Photocatalytic degradation of Methylene Blue using a mixed catalyst and product analysis by LC/MS. *Chem. Eng. J.* **157**, 373–378. https://doi.org/10.1016/j.cej.2009.11.017 (2010).
33. Asghar, A., Raman, A. A. A. & Daud, W. M. A. W. Advanced oxidation processes for in-situ production of hydrogen peroxide/hydroxyl radical for textile wastewater treatment: a review. *J. Clean. Prod.* **87**, 826–838. https://doi.org/10.1016/j.jclepro.2014.09.010 (2015).
34. Kumar, M. S., Sonawane, S. H. & Pandit, A. B. Degradation of methylene blue dye in aqueous solution using hydrodynamic Cavitation based hybrid advanced oxidation processes. *Chem. Eng. Process.* **122**, 288–295. https://doi.org/10.1016/j.cep.2017.09.009 (2017).
35. Vo, Q. V. et al. Reaction of methylene blue with OH radicals in the aqueous environment: mechanism, kinetics, products and risk assessment, RSC Adv. 14 https://doi.org/27265-27273.10.1039/D4RA05437G. (2024).
36. Zhang, H. F. et al. Study on transient characteristics and influencing of temperature on cavitation bubbles in various environments. *Optik* **187**, 25–33. https://doi.org/10.1016/j.ijleo.2019.01.076 (2019).
37. Orthaber, U. et al. Effect of laser-induced cavitation bubble on a thin elastic membrane. *Opt. Laser Technol.* **64**, 94–100. https://doi.org/10.1016/j.optlastec.2014.05.008 (2014).
38. Plesset, M. The dynamics of cavitation bubbles. *Appl. Mech.* **16**, 227–290. https://doi.org/10.1007/BF02120348 (1949).
39. Brennen, C. E. *Cavitation and Bubble Dynamics* (Oxford University Press, 1995). https://doi.org/10.1017/CBO9781107338760
40. Kim, K. Y., Byun, K. T. & Kwak, H. Y. Temperature and pressure fields due to collapsing bubble under ultrasound. *Chem. Eng. J.* **132**, 125–135. https://doi.org/10.1016/j.cej.2007.01.037 (2007).
41. Barbaglia, M. O. & Bonetto, J. F. Dependence on liquid temperature and purity of light emission characteristics in single cavitation bubble luminescence. *J. Appl. Phys.* **95**, 1756–1759. https://doi.org/10.1063/1.1637711 (2004).
42. Rayleigh, L. On the pressure developed in a liquid during the collapse of a spherical cavity. *Philos. Mag Ser.* **634** (200), 94–98. https://doi.org/10.1080/14786440808635681 (1917).

43. Kavitha, V. & Palanivelu, K. Destruction of cresols by Fenton oxidation process. *Water Res.* **39**, 3062–3072. https://doi.org/10.1016/j.watres.2005.05.011 (2005).
44. Sun, J. H. et al. A kinetic study on the degradation of p-nitroaniline by Fenton oxidation process. *J. Hazard. Mater.* **148**, 172–177. https://doi.org/10.1016/j.jhazmat.2007.02.022 (2007).
45. Vichare, N. P. et al. Energy analysis in acoustic cavitation. *Ind. Eng. Chem. Res.* **39**, 1480–1486. https://doi.org/10.1021/ie9906159 (2000).
46. Chakinala, A. G. et al. Industrial wastewater treatment using hydrodynamic cavitation and heterogeneous advanced Fenton processing. *Chem. Eng. J.* **152**, 498–502. https://doi.org/10.1016/j.cej.2009.05.018 (2009).
47. Wang, X. K. et al. Chemical effect of swirling jet-induced cavitation: degradation of rhodamine B in aqueous solution. *Ultrason. Sonochem.* **15**, 357–363. https://doi.org/10.1016/j.ultsonch.2007.09.008 (2008).
48. Merouani, S. et al. Sonochemical degradation of Rhodamine B in aqueous phase: effects of additives. *Chem. Eng. J.* **158**, 550–557. https://doi.org/10.1016/j.cej.2010.01.048 (2010).
49. Timberlake, G. T. et al. Free radical production by Nd:YAG laser photodisruption, Ophthal. *Surg. Las.* **28**, 582–589. https://doi.org/10.1016/S1060-1872(97)80040-8 (1997).

Acknowledgements

The authors are grateful to the projects supported by Natural Science Foundation of Nantong(JC2024035), Jiangsu Provincial Higher Education Natural Science General Project (24KJD610003), Natural Science Foundation of Jiangsu College of Engineering and Technology (GKYK/2024/2).

Author contributions

Xinxin Zhou: Conceptualization, Methodology, Investigation, Supervision, Writing - original draft.Jiayang Gu: Conceptualization, Supervision, Writing - review& editing.

Declarations

Competing interests

The authors declare no competing interests.

Ethical approval

This study does not involve human or animal subjects, and thus, no ethical approval is required. The study protocol adheres to the guidelines established by the journal.

Additional information

Correspondence and requests for materials should be addressed to J.G.